Preliminary In Vivo Validation of a Dedicated Breast MRI and Sonographic Coregistration Imaging System

Petrina A. Causer[1]
Cameron A. Piron[2]
Roberta A. Jong[1]
Donald B. Plewes[3]

OBJECTIVE. Sonographic correlation of breast MRI findings is often challenging. We present a preliminary in vivo feasibility study evaluating the degree of error of a new MRI–sonography coregistration system for showing MRI and sonographically visible breast lesions.

CONCLUSION. In 10 patients with 13 lesions, the system was found to be an accurate means for targeting sonography to MRI of the same breast lesions.

Keywords: breast cancer, MRI, sonography

DOI:10.2214/AJR.07.3495

Received December 4, 2007; accepted after revision April 20, 2008.

The coregistration system described in this article was developed by the Department of Imaging Research at the University of Toronto. The prototype is commercially available from Sentinelle Medical. C. A. Piron is president and a stockholder and D. B. Plewes is a stockholder in Sentinelle Medical.

Supported by a grant from the Terry Fox Foundation of the National Cancer Institute of Canada.

[1]Department of Medical Imaging, Sunnybrook Health Sciences Centre, University of Toronto, 2075 Bayview Ave., MG166, Toronto, ON, M4N 3M5, Canada. Address correspondence to P. A. Causer (Petrina.Causer@sunnybrook.ca).

[2]Sentinelle Medical, Toronto, ON, Canada.

[3]Departments of Imaging Research and Medical Biophysics, Sunnybrook Health Sciences Centre, University of Toronto, Toronto, ON, Canada.

AJR 2008; 191:1203–1207

0361–803X/08/1914–1203

Sonographic evaluation after breast MRI has become the standard method for attempting to identify mammographically occult MRI-detected lesions for several distinct purposes including lesions requiring characterization (BI-RADS category 0), lesions considered probably benign requiring imaging follow-up instead of biopsy (BI-RADS category 3), and indeterminate to suspicious lesions (BI-RADS categories 4 and 5) requiring biopsy [1]. Sonography, because it is less expensive and more readily available than MRI, is preferable for follow-up of BI-RADS category 3 lesions and remains the most desirable method of biopsy guidance [2, 3].

However, at evaluation after MRI–sonography, the target lesion may not be visualized. LaTrenta et al. [4] reported that only 21 of 93 (23%) mammographically occult MRI-detected lesions sent to sonography were sonographically visible. Even if a lesion is identified after MRI–sonography examination, it is often unclear whether that lesion corresponds to the MRI-detected lesion in question. MRI-guided breast biopsy is used with increasing frequency, particularly for biopsy of lesions that are visible only on MRI but are occult at mammography and conventional sonography. However, the limitations of MRI-guided procedures include the high costs of MRI-compatible disposables and time-consuming use of limited MRI resources.

Because the sampling is not performed under real-time visualization, as with sonography, and because it is not currently practical to image the sample with MRI to confirm retrieval of the targeted lesion as with stereotactic biopsy of calcifications, biopsy accuracy can be an issue in certain cases. As many as 4% of MRI-guided biopsies may miss the intended target [5].

To ensure that a suspicious lesion visible only on MRI is accurately sampled using sonographic guidance, previous in vitro work documented the accuracy of a coregistration system using sonography to locate an MRI-visible lesion in a breast phantom [6]. The purpose of this pilot study was to determine the accuracy of the same MRI–sonography coregistration system in vivo for showing breast lesions visible on MRI and sonography.

Subjects and Methods

Patients and Lesions

This prospective study was approved by the hospital institutional review board, and informed patient consent was obtained. The study was performed over a 1-year period. Ten women were recruited including eight women (age range, 43–75 years; mean age, 52.5 years) with 10 sonographically detected cysts and two women (mean age and age range, 50 years) with three masses detected at MRI screening. A total of 13 consecutive lesions were evaluated. By chance, all lesions were located centrally within the breast; there were none immediately subareolar or against the chest wall. Initial clinical indications for imaging patients included the diagnostic workup of a palpable or mammographic mass diagnosed as a simple cyst (n = 8) and screening patients at high risk for breast cancer (n = 2).

From the first cohort of women with breast cysts, lesions were diagnosed as simple cysts

on the basis of the sonographic features and confirmed on MRI. The three MRI-detected masses were classified as BI-RADS category 4 or 5 and were diagnosed by MRI-guided biopsy (n = 1) or sonography-guided biopsy (n = 2).

Breast MRI and Sonographic Coregistration Equipment

Both breast MRI and sonography were performed with the patient in the prone position using a system designed at our institution that featured a redesign of the MRI bed and coil system. The stretcher and supporting table design allowed open access to the medial and lateral breast to facilitate MRI-guided biopsy as previously described [7] or sonographic coregistration (Fig. 1). The mobile stretcher was designed for use with a 1.5-T magnet (Signa, GE Healthcare).

The breast was immobilized between medial and lateral compression frames containing a large open aperture, allowing the ultrasound transducer medial or lateral access to the breast through a thin sonography-compatible membrane (Fig. 1B). Fixation points on the frame allowed attachment and exchange of the MR receiver coils [8, 9] for the ultrasound transducer positioning stage (Fig. 1C). MRI-visible fiducial markers were set in known locations within the frame.

The stage positioned the transducer in three dimensions relative to the frame and the patient including x or superoinferior, y or anteroposterior, and z or depth from skin and with two 35° angles of freedom (elevation and azimuth), totaling 5 *df*. The 5 *df* of the stage position were calculated on the basis of the MRI coordinates of the lesion relative to the fiducial markers using a computer program.

MRI–Sonography Coregistration Procedure

A 1.5-T magnet (Signa, GE Healthcare) was used. Phased-array bilateral breast coils of our own institutional design were used. After multiplanar localizer images were obtained, T1-weighted spin-echo imaging for fiducial markers was performed with the following parameters: TR/TE, 350/14; matrix, 128 × 256; and field of view, 25 cm. Coronal T1-weighted 2D fast spoiled gradient-recalled echo (FSPGR) (150/4.2; flip angle, 50°; matrix, 256 × 256; and field of view,

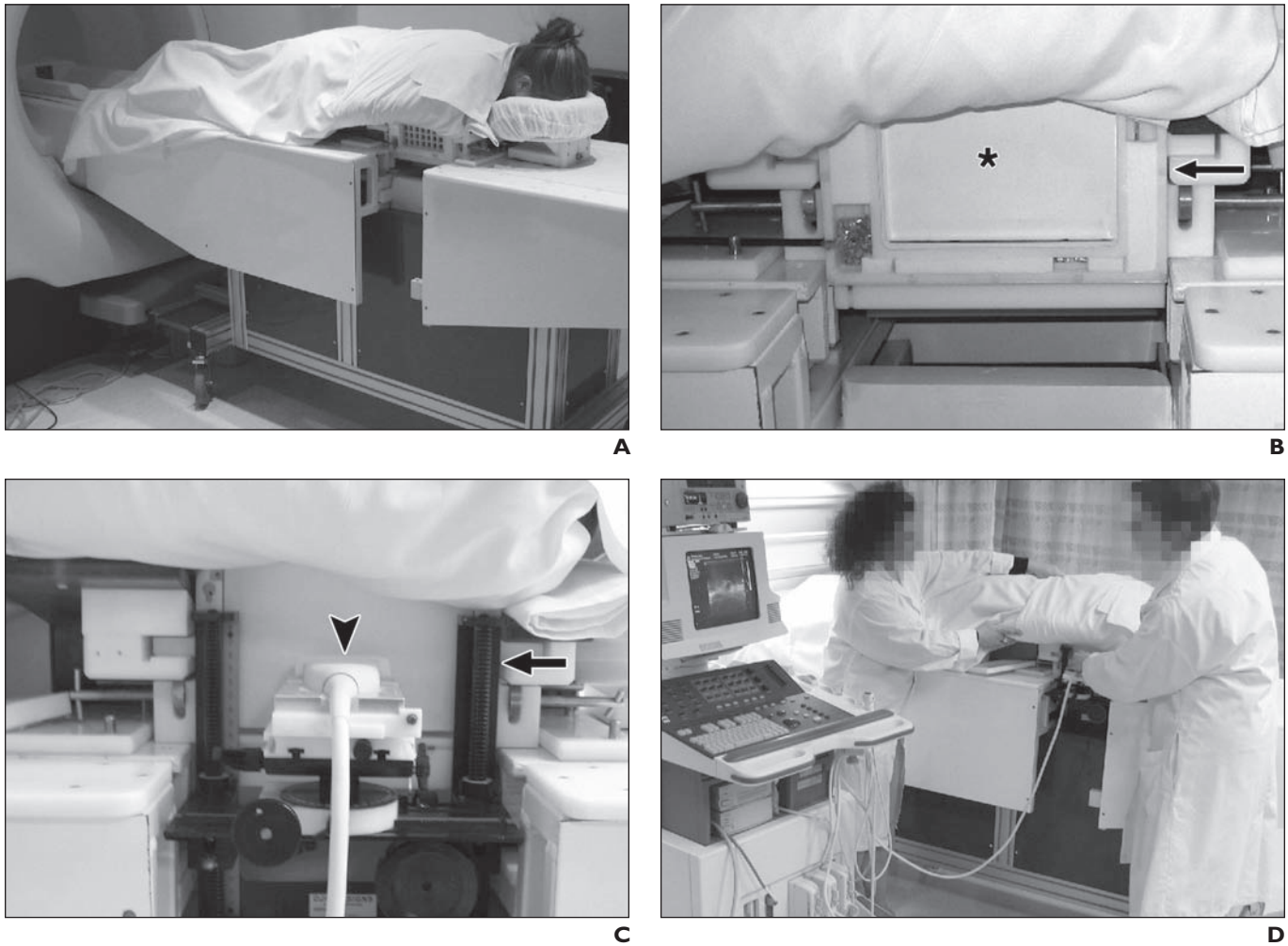

Fig. 1—MRI–sonography coregistration system, prepared for MRI and sonography.
A, Photograph shows redesigned patient support and breast imaging table set up for MRI. Table is docked in place of standard imaging table.
B, Photograph shows redesigned patient support and breast imaging table set up for MRI. Open aperture, covered by thin sonography-compatible membrane (*asterisk*), allows ultrasound transducer access to image breast. Breast MR receiver coil (*arrow*) is removable once MRI is complete.
C, Photograph shows MRI–sonography coregistration imaging system set up for sonography. Outside magnet, MR coil is exchanged for ultrasound transducer positioning stage (*arrow*). Once stage is set according to calculated 5 *df* based on position of MRI target lesion, ultrasound transducer is placed on stage (*arrowhead*).
D, Photograph shows patient undergoing sonography outside of magnet in private area.

20 cm) and sagittal unenhanced T2-weighted fast spin-echo fat-suppressed (3,000/102; matrix, 128 × 256; and field of view, 20 cm) sequences were then performed.

Additional imaging for masses included administration of 0.1 mmol/kg gadodiamide (Omniscan, GE Healthcare) by rapid injection. Three series of unenhanced sagittal T1-weighted 2D FSPGR fat-suppressed images followed by 11 series of contrast-enhanced images were performed with the following parameters: 150/4.2; flip angle, 50°; matrix, 128 × 256; field of view, 20 cm; and slice thickness, 3 mm. The scanning time for each series was 20 seconds. A sagittal T1-weighted 3D FSPGR fat-suppressed image was then obtained with the following parameters: 50/4.2; flip angle, 50°; matrix, 256 × 512; field of view, 20 cm; and slice thickness, 1 mm. The scanning time was 6 minutes 50 seconds. A final set of three dynamic series of delayed sagittal T1-weighted 2D FSPGR fat-suppressed images were then performed.

Once the target lesion was identified at the MR console, the lesion coordinates were obtained from the T2-weighted images for cysts or from the first contrast-enhanced T1-weighted 2D FSPGR fat-suppressed image in which a solid mass was visualized. The location of the lesion was determined from its MRI coordinates relative to the fiducial markers. A computer program was used to calculate the 5 *df* of the ultrasound transducer stage, which would allow the ultrasound beam to intercept the lesion of interest, displaying the lesion centered in the sonographic field of view. The calculation was based on lesion and fiducial marker coordinates.

Remaining in the same position atop the redesigned bed, patients were removed from the magnet room and taken to an adjoining private room to undergo sonography. The detachable MR breast coil was removed, Sonography coupling gel was applied liberally to the ultrasound transducer head and membrane, and the ultrasound transducer stage was attached to the compression frame (Figs. 1B and 1C).

Sonography was performed using a linear 5-12–MHz transducer (HDI 5000, Philips Healthcare). The transducer was placed in the stage, based on the MRI-predicted lesion location, according to the coordinates calculated with respect to the patient. The *x* (superoinferior), *y* (anteroposterior), and *z* (depth from skin) coordinates were dialed in as were the elevation and azimuth angles (Fig. 1C).

The coronal T1-weighted 2D FSPGR images served as a reference to correlate breast parenchymal patterns between MR images and sonograms and to calculate speed-of-sound variations through fat.

Data and Statistical Analyses

Lesion size in the *x* dimension was measured from the MR images and sonograms. The mean lesion size based on MRI and sonography was correlated using linear regression analysis.

In addition to lesion size and morphology, surrounding breast parenchymal interfaces and features were used to confirm that the same lesion was identified on both techniques (Figs. 2 and 3). Lesion pathology was determined on the basis of imaging features diagnostic of cysts or histopathology for masses.

Targeted lesions were displayed on the sonography monitor on the basis of the calculated transducer stage coordinates from the MR images (Figs. 2 and 3). For no error to be present, it was required that the sonogram of the targeted lesion appear centered on the sonography display monitor at a depth from the skin (*z* measurement) predicted by the computer calculation.

The true sonographic position error measurements were calculated in the *x* and *z* planes from the sonogram by determining the difference in the center of the displayed lesion coordinates and initial lesion center coordinates calculated on the basis of the MRI. This measurement was performed prospectively by placing a cursor on the sonography monitor at the MRI-predicted coordinates and measuring the distance to the sonography lesion center coordinates for both the *x* and *z* planes (Fig. 3B). If the target lesion was not immediately displayed, based on the calculated stage coordinates, the stage and ultrasound transducer were repositioned in the *y*-plane until the targeted lesion was displayed. The error measurement for the *y*-plane was then calculated on the basis of the difference in the initially predicted and the final repositioned stage positions.

Because the speed of sound differs in fat compared with soft tissue, there is an anticipated

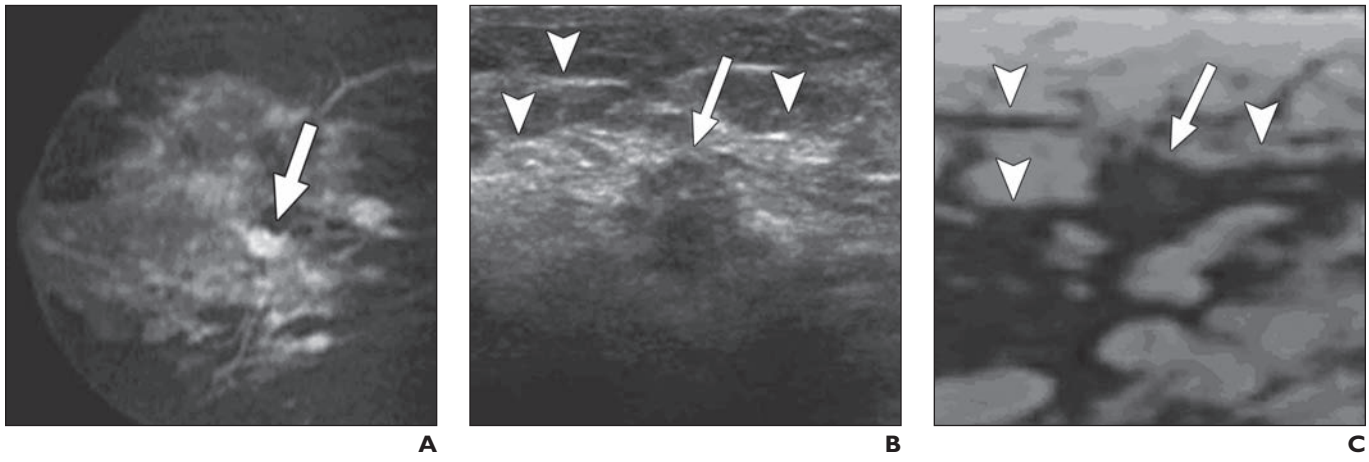

Fig. 2—MRI–sonography coregistration images in 50-year-old asymptomatic woman at high risk who presented with BI-RADS category 5 mass in left breast detected on MRI screening examination, corresponding to invasive ductal carcinoma.
A, Sagittal fat suppressed T1-weighted 2D spoiled gradient-recalled acquisition in steady-state MR image (TR/TE, 150/4.2) of left breast shows 9-mm enhancing lobulated mass with irregular margins (*arrow*) corresponding to target MRI mass lesion.
B, Coregistered coronal sonogram shows irregular mass (*arrow*) that is isoechoic to fat, with similar size and location from the MRI calculated position. Echogenic fibroglandular tissue interfaces with more hyperechoic fat surrounding mass are indicated by arrowheads and are similar to those visible on coronal MR image in **C**. Measured three-plane error from sonogram in this case was *x* error = 1.6 mm, *y* error = 1.8 mm, and *z* error = -1.4 mm.
C, Coronal T1-weighted 2D fast spoiled gradient-recalled echo MR image (150/4.2) shows same mass (*arrow*) as in **A** and **B**. Arrowheads indicate low-signal fibroglandular interfaces with surrounding high-signal-intensity fat and are similar to those indicated on sonogram in **B**. Breast parenchymal patterns were used in addition to similar mass size to ensure lesion correlation between sonography and MRI.

error in the *z*-plane. To correct for this error, we retrospectively measured the distance of fat between the skin surface and the lesion on the coronal T1-weighted MR image (Fig. 3C). On the basis of this measurement, a correction was calculated defined as the product of the sonographic propagation distance through fat and the ratio of the speed of sound through fat divided by the speed of sound in soft (fibroglandular) tissue, as previously described [6]. The initial *z*-plane error measurement was then recalculated based on this correction.

Results

The mean lesion size correlated well (R = 0.99) on MRI (11.4 mm; range, 6–28 mm) compared with sonography (10.3 mm; range, 6–28 mm). All three masses were invasive ductal carcinoma at histopathology.

The mean error measurements in the three planes were as follows: *x*-plane, 2.5 mm (range, 0.9–6.3 mm); *y*-plane, 1.1 mm (range, 0–4 mm); and *z*-plane, –2.6 mm (range, –0.9 to 5.3 mm). The mean sonographic speed of sound through fat correction value was 1 mm (range, 0.5–2.2 mm). After applying the correction value to the initially calculated *z*-plane error measurement, the *z*-plane error decreased to –1.7 mm (range, –0.04 to 4.2 mm).

Discussion

We have determined that our system allows accurate sonographic targeting of a breast lesion based on its MRI-identified position in the breast. With the added computer software assistance for calculating ultrasound transducer placement, the mean *x*, *y*, and *z* plane errors for displaying the MRI-targeted lesion with sonography were 2.5, 1.1, and –2.6 mm, respectively. Once a correction was calculated and applied, accounting for the distance of fat the ultrasound beam traversed to reach the lesion, the *z*-plane error decreased further to –1.7 mm.

The good correlation of the MRI and sonographic lesion size can be explained by the types of lesions included: focal masses and cysts. The reproducible size between the imaging studies was anticipated and was one factor used to ensure the same lesion was being documented. Breast parenchymal landmarks, including fat–fibroglandular interfaces visible on both MRI and sonography, are another useful means to ensure that the same MRI target area is shown with sonography.

Anticipated future clinical applications using this MRI–sonography coregistration system include roles in both diagnostic workup and biopsy guidance of MRI-detected lesions. One such application is to ensure that a sonographic finding corresponds to an MRI lesion in question when there is doubt using traditional supine sonography. Once a sonographic correlative lesion is confidently identified, it can be appropriately managed using sonographic guidance, including follow-up or biopsy.

An anticipated future use of this system is sonography-guided biopsy of an MRI-detected lesion. Even though MRI-guided percutaneous vacuum-assisted biopsy has become the standard of care for biopsy of suspicious lesions visible only on MRI or lesions for which a sonographic correlative lesion cannot be found with confidence, there is a small but real potential for sampling error. Prior studies that included relatively small numbers have found MRI-guided vacuum-assisted biopsy to be very accurate, with false-negative rates of 6% reported in an in vitro phantom study and ranging from 2% to 4% in vivo [5, 10–12]. However, in reality, imaging–histopathologic correlation and MRI follow-up are most often the only methods from which to infer accurate sampling of benign lesions. Often, on the basis of MRI, there is no direct evidence that the lesion has been accurately biopsied

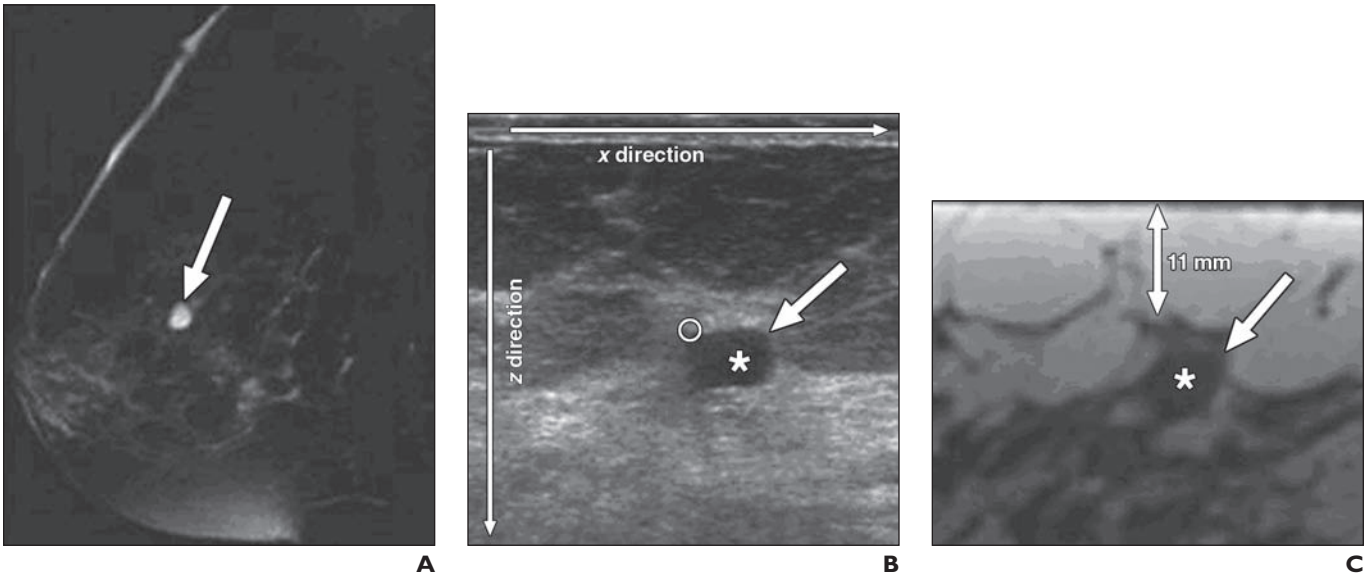

Fig. 3—MRI–sonography coregistration images in 65-year-old woman who presented initially with mass on mammography, confirmed as cyst on sonography.
A, Sagittal fat-suppressed T2-weighted fast spin-echo MR image (TR/TE, 3,000/102) of left breast shows 8-mm cyst (*arrow*) corresponding to target MRI lesion.
B, Coronal sonogram of MRI cystic target lesion (*arrow*), obtained by positioning ultrasound transducer and stage according to calculated stage position coordinates based on MRI; *x* (superoinferior with respect to the patient) and *z* (depth from skin) directions are shown on sonogram. Because lesion was anticipated to be centered in image, *x* and *z* measurement errors were measured on sonogram, taking difference between center of sonogram (*asterisk*) and actual center of lesion displayed (*circle*) in both directions. Registration error was measured in this case as $x = 4$ mm, $y = 1$ mm, and $z = 2.5$ mm.
C, Coronal T1-weighted 2D fast spoiled gradient-recalled echo MR image (150/4.2) of same cyst (*arrow*) as in **A** and **B**. Coordinates of center of cyst (*asterisk*) were obtained to calculate expected lesion position on sonography. In addition to lesion identification on both MRI and sonography, breast parenchymal interfaces on coronal sonograms and MR images (**B**) were identified to ensure lesion correlation. Amount of fat between lesion and skin surface was measured as 11 mm in this case, as shown, to calculate expected error introduced in *z*-plane by differential speed of sound through fat compared with fibroglandular tissue.

because of the small size or nature of the lesion and parenchymal enhancement, hematoma, and air introduced at the time of biopsy obscuring the target lesion. A previous report using a prototype of the MRI–sonography coregistration system used in this study for in vitro biopsy using a breast phantom reported a higher accuracy using sonography as the method of needle guidance for biopsy compared with MRI alone [6].

In addition to potentially improving sampling accuracy, the overall cost of the biopsy could be reduced by eliminating the need for expensive MR-compatible percutaneous devices. Also, because the biopsy would be performed outside of the magnet, efficiency of magnet use could be improved by the continued imaging of other patients during the biopsy.

One limitation of this study is the inability of other institutions to reproduce the study or results because this system is currently in development and not yet commercially available. However, this study was undertaken to confirm system accuracy before proceeding with further development. The small number of lesions included in the study is a further study limitation for evaluating both targeting error and the physical constraints of the system for lesion evaluation.

In conclusion, our system offers an accurate means for targeting sonography to MRI of the same breast lesions. Currently, this system enables confident identification of a sonographic correlate to an MRI lesion for lesions visible on sonography. As the targeting accuracy of the system is confirmed, further system development can proceed, including a sonographically guided biopsy mechanism using this system for lesions visible only on MRI.

Acknowledgment

We thank Joan Glazier for her valuable contribution in patient recruitment.

References

1. American College of Radiology. BI-RADS: ultrasound. In: *Breast imaging reporting and data system: BI-RADS atlas*, 4th ed. Reston, VA: American College of Radiology, 2003
2. Mainiero MB, Gareen IF, Bird CE, Smith W, Cobb C, Schepps B. Preferential use of sonographically guided biopsy to minimize patient discomfort and procedure time in a percutaneous image-guided breast biopsy program. *J Ultrasound Med* 2002; 21:1221–1226
3. Liberman L, Feng TL, Dershaw DD, Morris EA, Abramson AF. US-guided core breast biopsy: use and cost-effectiveness. *Radiology* 1998; 208:717–723
4. LaTrenta LR, Menell JH, Morris EA, Abramson AF, Dershaw DD, Liberman L. Breast lesions detected with MR imaging: utility and histopathologic importance of identification with US. *Radiology* 2003; 227:856–861
5. Lee JM, Kaplan JB, Murray MP, et al. Imaging histologic discordance at MRI-guided 9-gauge vacuum-assisted breast biopsy. *AJR* 2007; 189:852–859
6. Piron CA, Causer P, Jong R, Shumak R, Plewes DB. A hybrid breast biopsy system combining ultrasound and MRI. *IEEE Trans Med Imaging* 2003; 22:1100–1110
7. Causer PA, Piron CA, Jong RA, et al. MR imaging-guided breast localization system with medial or lateral access. *Radiology* 2006; 240:369–379
8. Warner E, Plewes DB, Hill KA, et al. Surveillance of BRCA1 and BRCA2 mutation carriers with magnetic resonance imaging, ultrasound, mammography, and clinical breast examination. *JAMA* 2004; 292:1317–1325
9. Koyner NB, Ramsay EA, Bronskill MJ, Plewes DB. Comparison of MR imaging breast coils. *Radiology* 2002; 222:830–834
10. Lehman CD, Aikawa T. MR-guided vacuum-assisted breast biopsy: accuracy of targeting and success in sampling in a phantom model. *Radiology* 2004; 232:911–914
11. Orel SG, Rosen M, Mies C, Schnall MD. MR imaging-guided 9-gauge vacuum-assisted core-needle breast biopsy: initial experience. *Radiology* 2006; 238:54–61
12. Liberman L, Bracero N, Morris E, Thornton C, Dershaw DD. MRI-guided 9-gauge vacuum-assisted breast biopsy: initial clinical experience. *AJR* 2005; 185:183–193